ELSEVIER

Catalysis Today 76 (2002) 91–101

CATALYSIS TODAY

www.elsevier.com/locate/cattod

A novel preparation of high surface area TiO_2 nanoparticles from alkoxide precursor and using active carbon as additive

G. Colón*, M.C. Hidalgo, J.A. Navío

Instituto de Ciencia de Materiales de Sevilla, Centro Mixto CSIC, Universidad de Sevilla, Américo Vespucio s/n, 41092 Sevilla, Spain

Abstract

TiO_2 nanoparticles have been prepared by a novel alkoxide sol–gel precipitation. The presence of active carbon in different percentages could act as an interesting template. Upon calcination, carbon is eliminated leaving surface features significantly different from TiO_2 prepared in the absence of carbon. Wide surface and structural characterisation of samples have been carried out. Correlations with carbon percentage is pointed out from this characterisation. Interesting spherical aggregates of nanosized TiO_2 are observed from TEM images probably stabilised by the presence of carbon. Physicochemical correlations made will be very useful in further application of these TiO_2 to be used as potential high surface area photocatalyst.

Keywords: TiO_2; Active carbon; Alkoxide; Sol–gel; Photocatalyst

1. Introduction

There is extensive experimental evidence that supports the notion that efficiency of photocatalytic reactions is strongly affected by one or more morphological parameters of the catalyst [1–9]. Several authors [2,3,8] have reported the simultaneous need to optimise mass transport and adsorption of reactants requires morphology of pore structure. The impact of nanostructure on the properties of high surface area materials is an area of increasing importance for understanding, creating and improving materials for diverse applications. A unique property of nanoparticles is their extremely high surface area. The synthesis of nanoparticles with controlled size and composition is of technological interest. In particular, there has been a lot of highlighting on the production of nanoparticulated TiO_2 for a wide range of applications. The photocatalytic activity of TiO_2 powder strongly depends on its microstructural and physical properties. In this sense, we have previously reported [10] that a tentative explanation for the surprising highest deactivation of commercial TiO_2 Degussa with respect to Hombikat one, used in a simultaneous photodegradation of Cr(VI) and salicylic acid, could be the different surface area and pore distribution of the commercial oxides. For this reason, many authors [11–14] have investigated the relationship between the synthesis conditions and the properties of nanosized TiO_2 powder, such as surface area, total pore volume, particle and pore size distribution, crystallinity, thermal stability, phase composition, etc. Synthetic routes for TiO_2 are usually based on a sol–gel precipitation from alkoxide precursors, producing an amorphous powder that upon calcination leads to TiO_2 generally in the anatase phase. This phase is generally assumed as the most active phase in photocatalytic processes.

* Corresponding author.
E-mail address: colon@cica.es (G. Colón).

0920-5861/02/$ – see front matter
PII: S0920-5861(02)00207-9

In the present paper, we deal with the preparation of TiO_2 following a standard sol–gel synthetic route from alkoxide precursor but introducing active carbon as template. The utilisation of organic molecules as polyethyleneglycol (PEG) or polyamides as templates [15–17], for controlling surface area and pore distribution is well known. In this case, we use high surface area activated carbon in the preparation of TiO_2. Recently, it has been reported that activated carbon have an interesting effect on the photocatalytic activity of TiO_2, since it increases the adsorption of organic pollutants to be photodegraded [18]. In our case, the effect of carbon is regarded in the preparation of the TiO_2 powders, and its effect on its surface and morphological properties.

2. Experimental

First series of TiO_2/C samples were prepared by means of a sol–gel precipitation from alkoxide precursor. Certain amount of active carbon Darco® KB, 100 mesh and 1400 m^2/g (supplied by Aldrich) were settled in ethanol suspension and then different volumes of $Ti(OiPr)_4$ (TIP, Aldrich 97%) were added. Samples were named as TiO_2/C *X*%. The indicated percentages (20, 40 and 80%) correspond to the weight percentage of final TiO_2 obtained with respect to initial carbon content. Once the suspension was homogenous, same volume of water was added. Precipitation was achieved by pouring down NH_4OH till pH was about 9. Coprecipitation samples were prepared in two series depending on the carbon weight/total volume ratio (5/100 and 5/200), named as COP I and COP II, respectively. A third series of samples was prepared by wet impregnation method (IMP series). In this case, TIP solution in ethanol was slowly pouring down over the stoichiometric amount of active carbon. In both cases, samples were dried at 110 °C during night and then calcined at 450 °C for 3 h. TiO_2 was also prepared following the same sol–gel precipitation procedure but in the absence of activated carbon in order to establish certain correlations with its effect in the structural and textural properties of TiO_2.

BET surface area measurements were carried out by N_2 adsorption at 77 K using a Micromeritics 2000 instrument. Pore volumes were determined using the cumulative adsorption of nitrogen by the BJH method.

Thermal evolution of the samples under dynamic conditions was studied by differential thermal and thermogravimetric analysis (DTA–TGA). These curves were obtained simultaneously in static air with a Sll Seiko instrument Exstar 6000, model TG/DTA6300 at a heating rate of 5 °C/min. Calcined alumina was used as reference material.

Carbon content on calcined samples has been analysed by means of a elemental analyser LECO CHNS-932. Carbon content was determined by means of infrared absorption. Sensitivity for C was 0.001%.

X-ray diffraction (XRD) patterns were obtained using a Siemens D-501 diffractometer with Ni filter and graphite monochromator. The X-ray source was Cu Kα radiation. From the line broadening of corresponding X-ray diffraction peaks, according to the Warren and Averbach equation (peaks were fitted by using a Voigt function):

$$D = \frac{\lambda\, 180}{\pi(\cos\theta)L}$$

where L is the line width at medium height, λ the wavelength of the X-ray radiation 0.15406 nm and θ the diffracting angle.

UV-Vis spectra were recorded in the diffuse reflectance mode (R) and transformed to a magnitude proportional to the extinction coefficient (K) through the Kubelka–Munk function, $F(R8)$.

Table 1
BET surface area and average pore size distribution for TiO_2 samples

Samples	COP I		COP II		IMP	
	S_{BET} (m^2/g)	Pore size diameter (Å)	S_{BET} (m^2/g)	Pore size diameter (Å)	S_{BET} (m^2/g)	Pore size diameter (Å)
TiO_2/C 20%	89	35/100	117	35/95	70	35/80
TiO_2/C 40%	74	72	80	35/90	58	35/85
TiO_2/C 80%	72	35/75	64	35/90	64	40/75/100
TiO_2	13	35/500	–	–	–	–

Scanning electron microscopy (SEM) was performed on gold-coated samples using a Jeol apparatus (model JSM-5400) and the dispersion of X-ray was measured with a Link Isis Model analyser; a semi-automatic image analyser of magnetostrictive Kontron MOP-30 board was used to estimate the average weight size of aggregates and particles.

Samples were also studied by transmission electron microscopy (TEM) using a Philips CM200 instrument. The microscope was equipped with a top-entry holder and ion pumping system, operating at an accelerating voltage of 200 kV and giving a nominal structural resolution of 0.21 nm. Samples were prepared by dipping a 3 mm holey carbon grid into ultrasonic dispersion of the oxide powder in ethanol.

3. Results and discussion

In Table 1 are summarised the surface area and average pore size for TiO_2 samples. From the results shown, it is clear that the sol–gel precipitation of TiO_2 in the presence of active carbon leads to a significantly higher surface area with respect to TiO_2 obtained in the absence of it (up to 10 times higher). TiO_2 obtained by a sol–gel precipitation route without using active carbon leads a relatively low surface area of 13 m^2/g. For samples prepared in the presence of active carbon S_{BET} are in all cases higher than 60 m^2/g, reaching in certain cases surface areas higher than 110 m^2/g. Furthermore, surface area values seem to follow a certain correlation with C/TIP ratio. The higher carbon percentage, the higher is the surface area. Thus, this increase in the surface area is directly related with the carbon used in the precipitation. This fact is more evident in the case of COP II samples, for which a higher precipitation volume has been employed (200 ml). Thus, for TiO_2 (20%) COP II a surface area higher than 110 m^2/g has been obtained; 10 times higher than that obtained for TiO_2 in the absence of active carbon. On the other hand, for TiO_2 IMP samples, prepared by impregnating TIP onto carbon, specific surface areas ranged between 60 and 70 m^2/g, with no apparent relation with the C/TIP fraction. Impregnation method seems to produce certain heterogeneous system with respect to carbon content, in terms of the surface properties (surface area, pore size distribution, etc.) of obtained TiO_2.

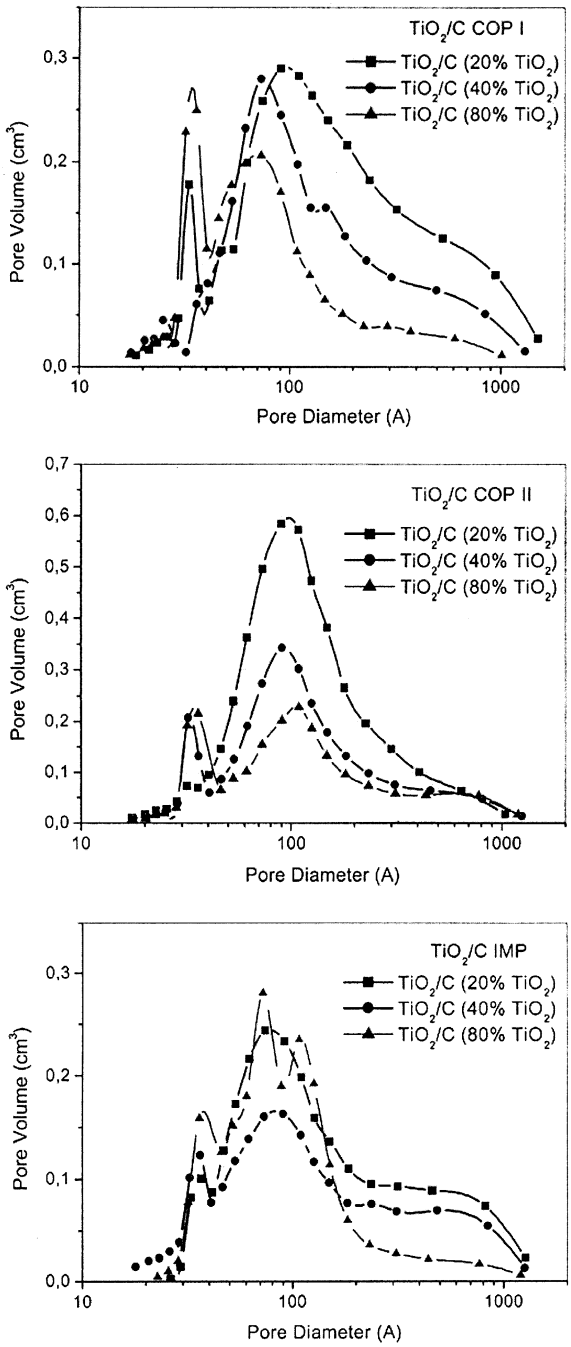

Fig. 1. Pore size distribution obtained from N_2 adsorption isotherms for TiO_2/C samples calcined at 450 °C.

Regarding the pore size distribution, Fig. 1 shows the evolution of this feature with the C content for the three series. In general, two clear pore families are observed (except in the case of TiO_2 80% IMP for which three pore size families can be found). One family with an average pore size of about 35 Å, and a second with an average size of 100 Å (Table 1). This pore size family could be related with the pore distribution of fresh active carbon, for which only one pore family is observed in this range. It can be also observed in the case of COP I samples a slight shift towards higher sizes in the second family of pores as C content is higher, appearing a new set of pores in the range of macropores. At the same time, the 35 Å family seems to decrease. For COP I series similar effect it is observed, there is no shift towards macropores, but the 35 Å pores almost disappear as C content increases. TiO_2 IMP series presents a heterogeneous distribution of pores but in any case same tendency as other two series can be noticed.

From thermal analysis of samples we obtain information about the evolution of TiO_2/C system during calcination. Fig. 2 shows the thermogravimetric diagrams of different samples. Weight losses are in all cases proportional with the carbon content of samples, and independent of the preparation method followed. Thus, depending on the carbon content weight losses values are about 52, 67 and 78% for carbon percentages 20, 40 and 80%, respectively. It is worthy to note that fresh precursor obtained in the sol–gel precipitation of TIP in the absence of active carbon leads to a total weight loss of about 20%. Total weight loss is observed in any case up to 550 °C indicating that whole carbon is eliminated before this temperature. From TG curves, it can be noticed that there is two important weight loss process corresponding to TIP alkoxide and carbon decomposition. The first one is located for all samples at around 400 °C, while carbon elimination takes place at slightly higher temperatures, ranged between 430 and 500 °C. Table 2 shows the carbon content of samples calcined at 450 °C obtained from elemental analysis. In all cases,

Table 2
Residual carbon content (%) in the prepared TiO_2 samples after calcination

Samples	COP I	COP II	IMP
TiO_2/C 20%	0.295	0.246	0.287
TiO_2/C 40%	0.255	0.319	0.279
TiO_2/C 80%	0.175	0.198	0.349
TiO_2	0.137	–	–

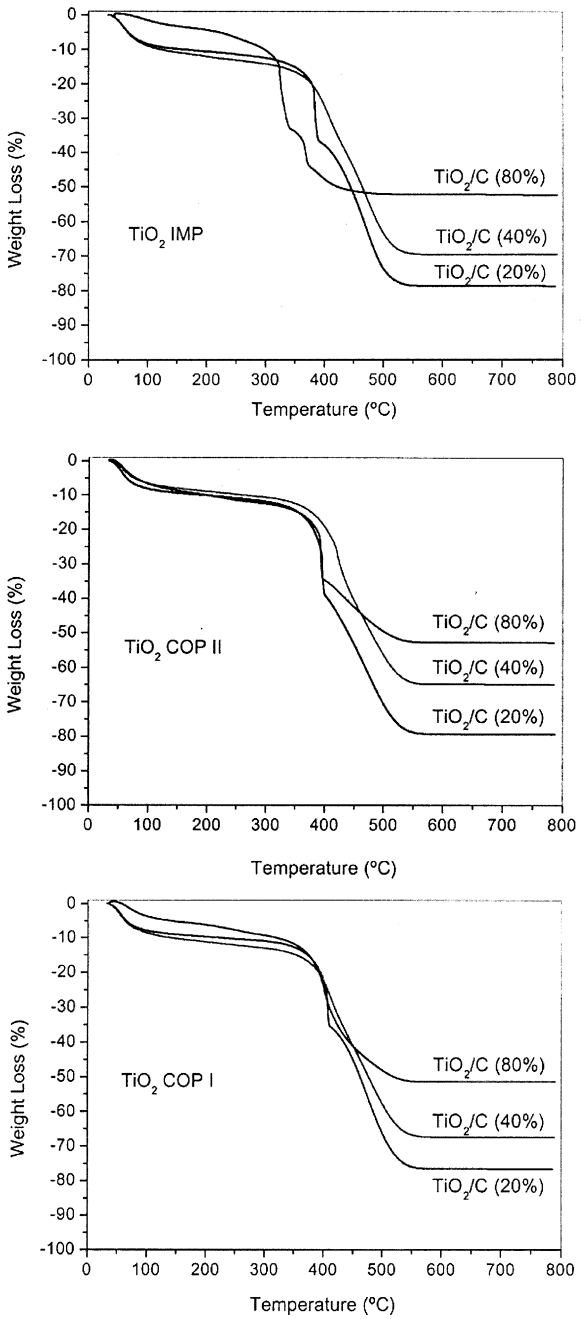

Fig. 2. Weight loss curves for TiO_2/C fresh samples.

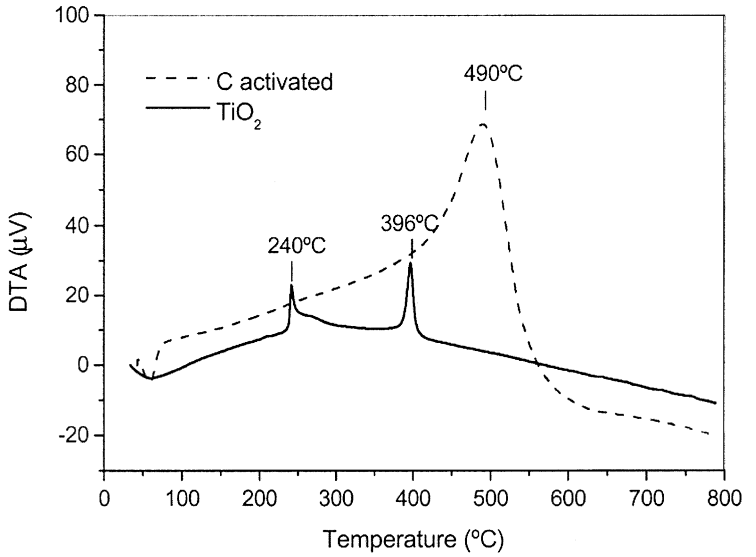

Fig. 3. DTA curves for TiO_2 precursor from TIP in the absence of active carbon, and active carbon itself.

residual carbon content measured from elemental analysis of samples is lower than 0.5% independently of the initial carbon present. This result indicates that practically all the active carbon has been eliminated upon calcination independently on the initial carbon content or the preparation route.

Fig. 3 depicts the DTA of TiO_2 gel precursor obtained in the absence of active carbon, and of active carbon itself. As it was stated from TG curves, the first weight loss observed (around 240 °C) should correspond to TIP decomposition, that is elimination of organic rest from alkoxide, showing a sharp exothermic

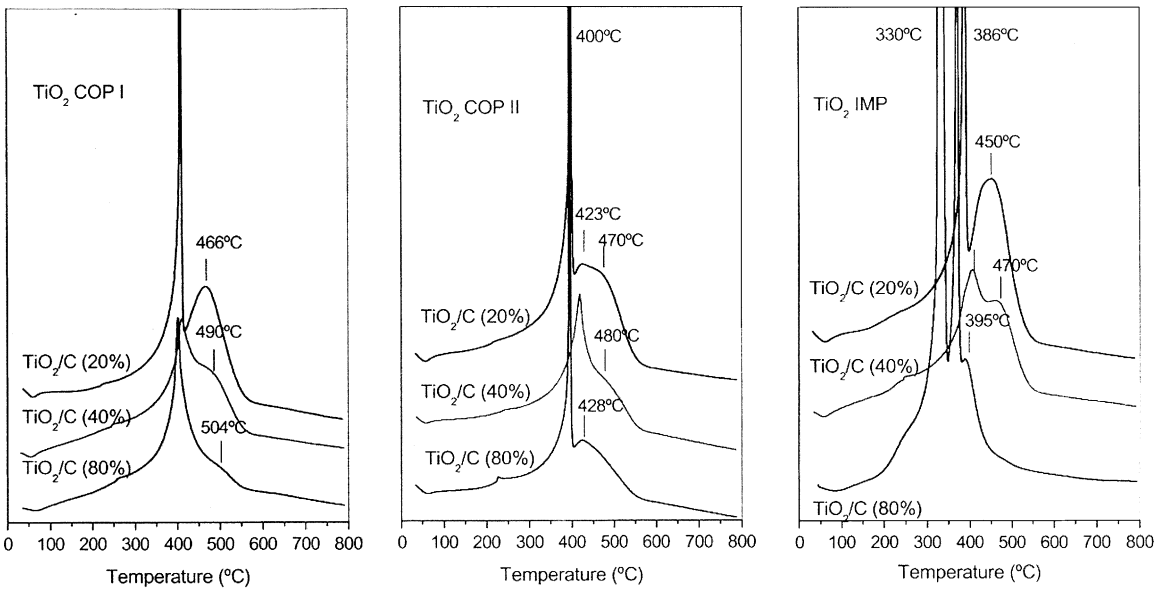

Fig. 4. DTA curves for TiO_2/C fresh samples.

Table 3
Crystallite size (nm) calculated form XRD for TiO_2 samples

Samples	COP I	COP II	IMP
TiO_2/C 20%	13	13	17
TiO_2/C 40%	14	16	16
TiO_2/C 80%	14	17	17
TiO_2	22	–	–

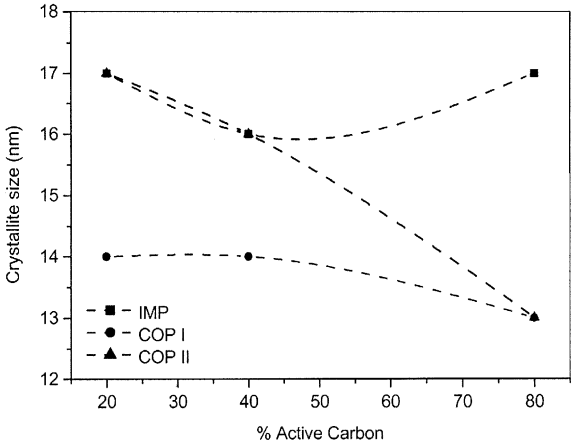

Fig. 5. Variation of the crystallite size calculated from XRD peak broadening with the carbon content.

peak. While the second exothermic effect located at around 400 °C should correspond to TiO_2 crystallisation. Regarding the fresh commercial carbon, elimination by combustion process occurs at slightly higher temperature, as it can be seen from the wide exothermic peak at 490 °C. DTA curves for TiO_2/C samples (Fig. 4) present a quite complex mixture of both previous curves. Anyway it can be observed for all cases at least two clear exothermic effects, and its relative intensities can be correlated with the TIP/C ratio.

Table 4
Band-gap values calculated for UV-Vis spectra for TiO_2 samples

Samples	COP I	COP II	IMP
TiO_2/C 20%	3.55	3.38	3.57
TiO_2/C 40%	3.42	3.39	3.42
TiO_2/C 80%	3.34	3.34	3.35
TiO_2	3.29	–	–

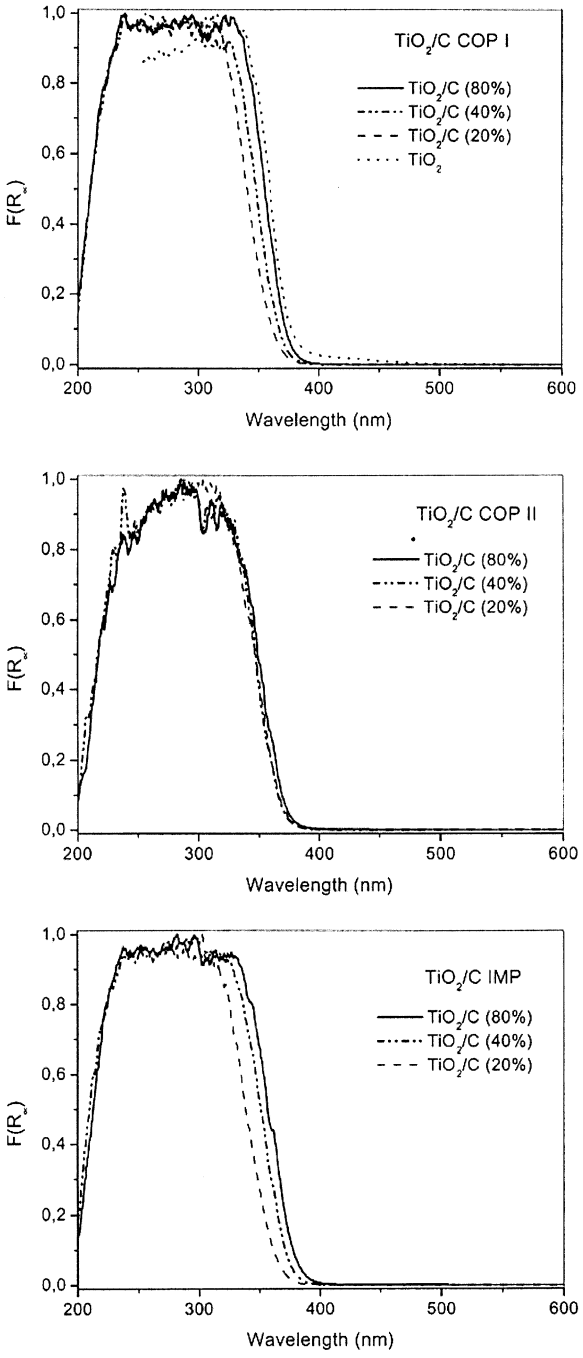

Fig. 6. UV-Vis diffuse reflectance spectra for TiO_2/C samples calcined at 450 °C.

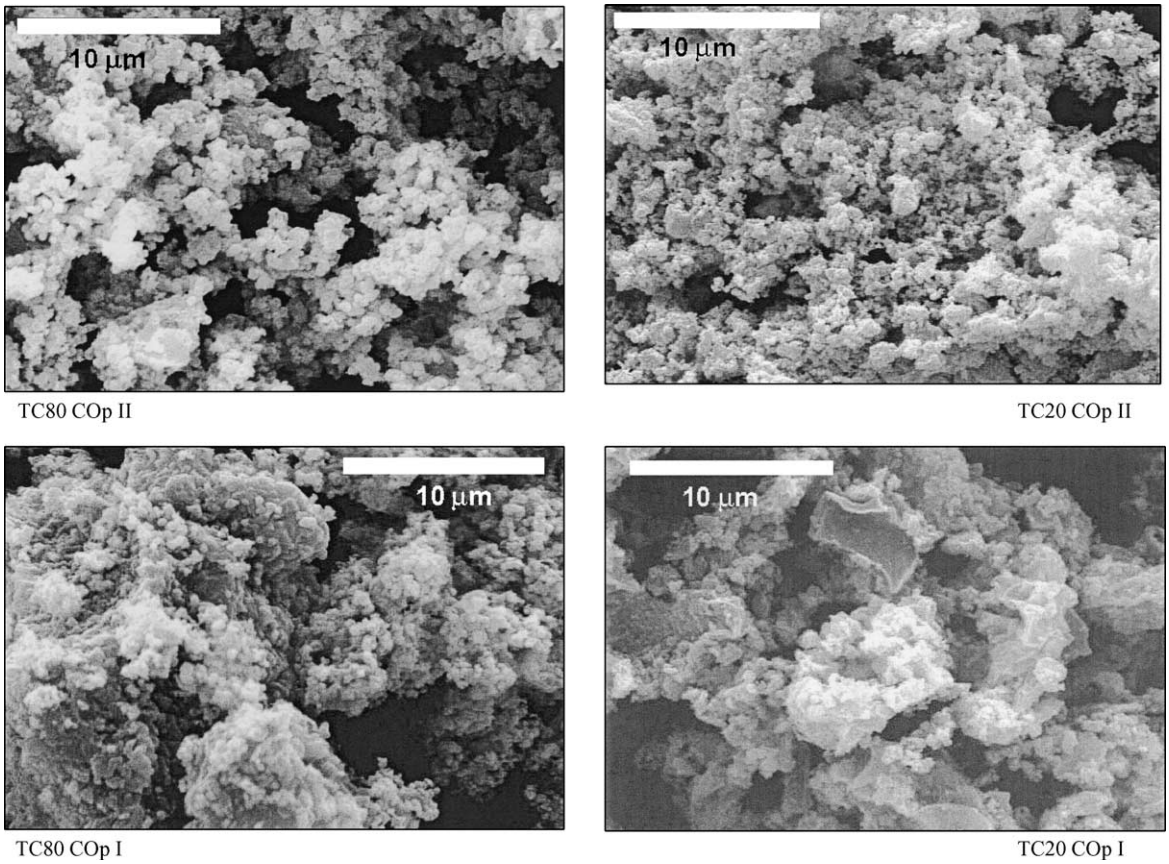

Fig. 7. Selected SEM images of TiO_2/C COP samples calcined at 450 °C.

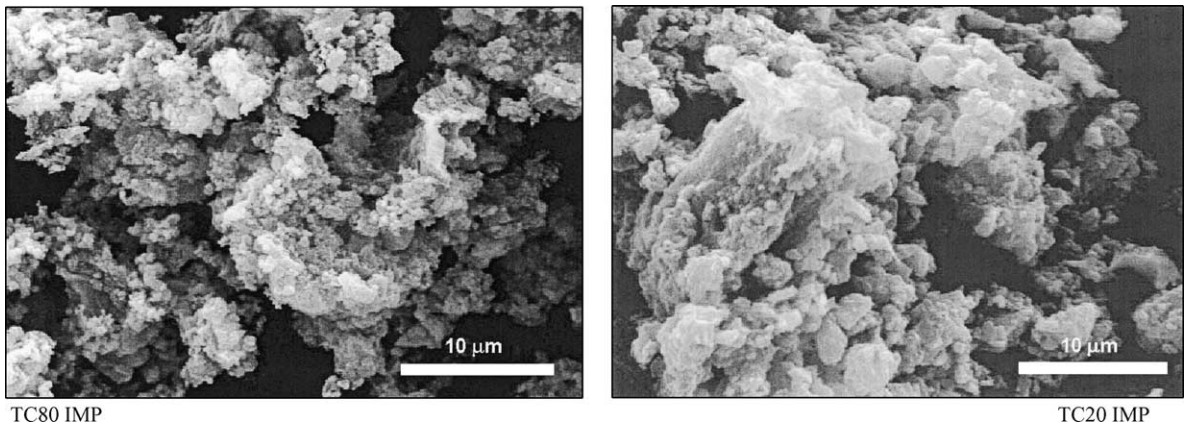

Fig. 8. Selected SEM images of TiO_2/C IMP samples calcined at 450 °C.

Upon calcination at 450 °C all TiO_2 samples present one crystalline anatase phase observed by XRD (result not shown). In Table 3 we summarise calculated mean crystallite size for TiO_2/C samples studied. It is worth noting that the mean crystallite size calculated by using the Scherrer equation seems to be related with the preparation procedure, especially in the coprecipitation method. TiO_2 obtained in the absence of carbon present a mean crystallite size of 22 nm. On the other hand, TiO_2/C samples present in all cases smaller crystallite sizes, especially those obtained from COP I method. Furthermore, it seems that the C percentage ratio has also certain influence in the crystallite size in the COP II series. Thus, the higher the carbon content, the lower is the crystallite size. This point is in agreement with BET results. As crystallite size decreases, the specific surface area becomes higher. This is the case of TiO_2 (20%) prepared by the COP II method, for which surface area was the highest. For samples obtained by the impregnation method, mean crystallite size calculated from XRD is in all cases around 14 nm, showing no influence with the carbon percentage. Fig. 5 clearly shows the influence of carbon content as well as preparation procedure in the crystallite size of calcined systems. Generally, for COP I and II series crystallite size seems to decrease as carbon content increases, that is TiO_2/C (20%) samples. For IMP series no clear tendency can be drawn from the variation of crystallite size versus carbon percentage. Regarding the preparation procedure, TiO_2/C systems from COP I series exhibit a slight increase in the crystallite size, while for COP II the variation is significantly higher as carbon percentage is lower.

Diffuse reflectance spectroscopy gives information about the electronic absorption of the material, and therefore the band-gap energy of the semiconductor can be estimated. This is an interesting feature of semiconductor to be used in photocatalytic applications. In Fig. 6 we show the UV-Vis diffuse reflectance spectra of TiO_2/C samples prepared from different series and calcined at 450 °C. In all cases, band-gap energies, ranged from 3.3 to 3.5 eV (Table 4). Absorption is produced in both cases at wavelength lower than 400 nm. Differences in the band-gap value could be

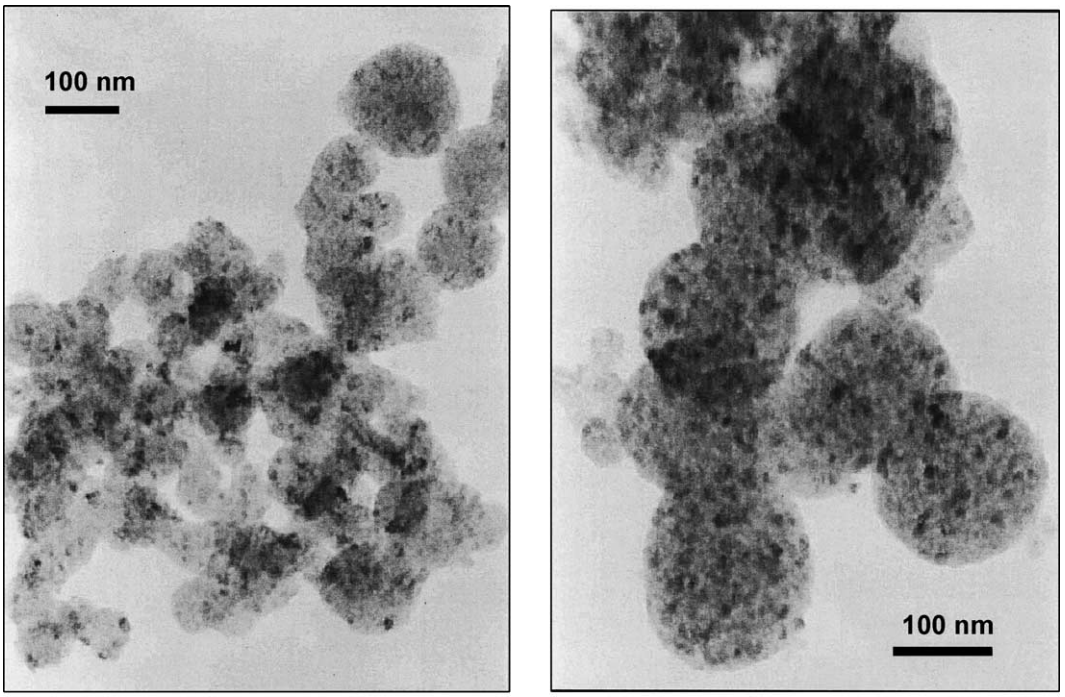

TC20 COP I TC80 COP I

Fig. 9. Selected TEM images of TiO_2/C COP I samples calcined at 450 °C.

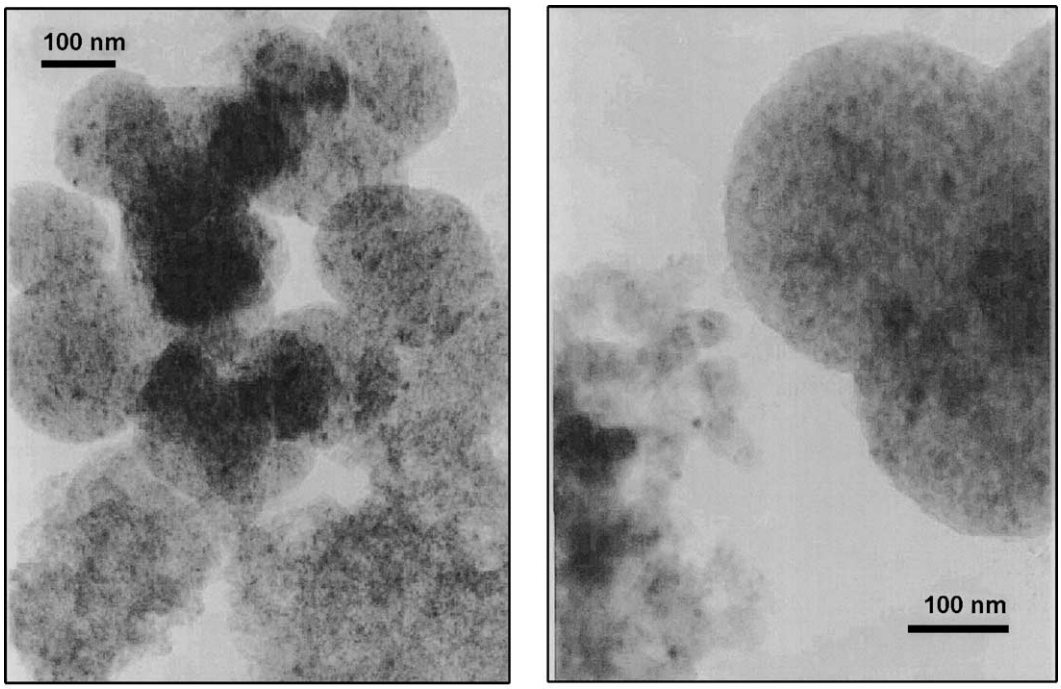

Fig. 10. Selected TEM images of TiO_2/C COP II samples calcined at 450 °C.

attributed to the different crystallite size, presence of crystallite defects or morphology.

Regarding to the TiO_2/C morphologies, SEM images clearly point out the homogeneity in shapes for all samples. In Figs. 7 and 8 are shown selected SEM images for TiO_2/C form different series. Morphologies of TiO_2/C samples prepared by coprecipitation method are quite homogeneous in shapes, as it can be inferred from SEM images (Fig. 7). They consist mainly in round particles. Interesting correlations can be established between the morphology and the carbon content in COP series. Thus, it seems that for COP II series particles are more homogenous in shapes that in the case of COP I. Additionally, it is clear that for samples with higher carbon content (TiO_2/C 20%) particles present significantly smaller diameter than those with lower carbon percentages. Hence, for 20% COP II particles appear with an average less than 1 mm diameter. On the other hand, IMP series samples (Fig. 8) present an heterogeneous and more irregular morphology. Indicating that in this preparation procedure, impregnation is not homogeneous along the carbon surface, leading after calcination to this irregular morphology material.

Effect of carbon addition on the preparation is more evident from TEM images (Figs. 9 and 10). Active carbon produces a template effect in the crystallite morphology. We have stated from XRD that crystallite sizes are in the range of nanometers (14–18 nm). Sol–gel precipitation in the presence of active carbon leads to regular spherical aggregates, around 90 nm diameter, formed by small particles of about 15 nm. They present a very homogeneous size distribution as can be seen from Fig. 9. Surprisingly, in the TiO_2/C (80%), two kinds of particles can be found. On one side, the typical spheres constituted by small crystallites, and on the other segregated roundish particles with higher crystallite size (20–30 nm). For TiO_2/C (20%), only spherical aggregates can be found. This fact indicates that the presence of active carbon stabilises the small nanometer crystalline particles forming these spherical particles. When active carbon is in a lower percentage certain fraction of TiO_2 nuclei crystallise forming these segregated particles of

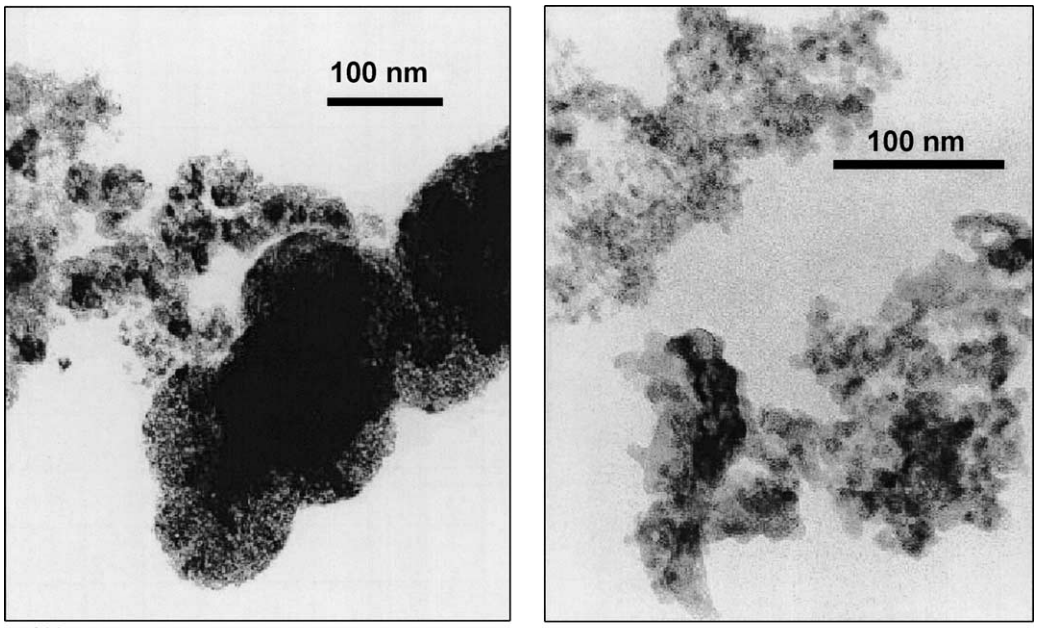

Fig. 11. Selected TEM images of TiO_2/C IMP samples calcined at 450 °C.

higher crystallite size. Therefore, the particular spherical shape can directly be attributed to the presence of activated carbon. That is the reason of the higher surface area exhibited by TiO_2/C (20%), especially in the COP II series. Similar concept was employed for the preparation of Ni nanoparticles encapsulated in carbon [19]. In that case carbon acted as protection environment against oxidation, as well as stabilising Ni as nanoparticles, avoiding nucleation and the formation of clusters.

For impregnated series, TEM images (Fig. 11) show clear different morphologies for all samples with respect to coprecipitation prepared ones. In this case, the spherical aggregates of particles are not found, though small crystallite size is still observed for this series, being in agreement with crystallite size distribution from XRD shown in Fig. 5.

4. Conclusions

Sol–gel precipitation of TiO_2 from alkoxide precursor in the presence of active carbon is a novel and suitable method for preparing high surface area nanometer TiO_2. Calcination at 450 °C practically eliminates the whole carbon from the fresh powder, leading to a nanosized anatase TiO_2. Surface areas of calcined TiO_2 are significantly higher with respect to the value observed for TiO_2 obtained by the single precipitation sol–gel route (without active carbon). Variations in the carbon content as well as in the C/solution volume affect remarkably in the surface area and morphology of samples. Therefore, this would be an interesting new preparation method for obtaining nanosized materials with homogeneous morphology. Impregnation method does not improve the surface and morphological properties of TiO_2 samples with respect to coprecipitation one, however high surface areas are also obtained.

Acknowledgements

This research was partially financed by FEDER (project ref. 1FD97-0340) and Ministerio de Ciencia y Tecnología (project ref. BQU2001-3872-C02-01). We also thank the financial support by the CYTED network (VIII-G, Spain).

References

[1] H. van Damme, Microheterogeneous systems, in: M. Gratzel, K. Kalyanasundaram (Eds.), Kinetics and Catalysis, Marcel Dekker, New York, 1991.
[2] D. Avnir, O. Citri, D. Farin, M. Ottolenghi, A. Seri-Levy, in: P.J. Plath (Ed.), Optimal Structures in Heterogeneous Reaction Systems, Springer, Berlin, 1990.
[3] D. Farin, J. Kiwi, D.J. Avnir, J. Phys. Chem. 93 (1989) 5851.
[4] D. Farin, J. Kiwi, D.J. Avnir, J. Phys. Chem. 95 (1991) 6100.
[5] D. Avnir, D. Farin, P. Pfeifer, Nature 308 (1984) 261.
[6] N. Serpone, M. Linder, E. Pelizzetti, in: E. Pelizzetti (Ed.), Fine Particles Science and Technology. From Micro to Nano Particles, Reidel, Dordrecht, 1996, p. 657.
[7] M. Anpo, T. Kawamura, S. Kodema, K. Maruya, T. Onshi, J. Phys. Chem. 92 (1988) 92.
[8] M. Tonikiewicz, G. Dagan, Z. Zhu, Res. Chem. Intermediates 20 (1994) 701.
[9] M. Toínkiewicz, S. Kelly, in: E. Pelizzetti (Ed.), Fine Particle Science and Technology From Micro to Nano Particles. Reidel, Dordrecht, 1996, p. 403.
[10] G. Colón, M.C. Hidalgo, J.A. Navío, J. Photochem. Photobiol.: A Chem. 138 (2001) 79.
[11] K.M. Reddy, C.V. Gopal, S.V. Manorama, J. Solid State Chem. 158 (2001) 180.
[12] S. Gablenz, D. Vbltzke, H.P. Abicht, J. Neumann-Zdralek, J. Mater. Sci. Lett. 17 (1998) 537.
[13] M. Ivanda, S. Music, S. Popovie, M. Gotic, J. Mol. Struct. 480–481 (1999) 645.
[14] Q. Zhang, L. Gao, J. Guo, Appl. Catal. B: Environ. 26 (2000) 207.
[15] K. Srikanth, M.M. Rahman, H. Tanaka, K.M. Krishna, T. Soga, M.K. Mishra, T. Jimbo, M. Umeno, Solar Energy Mater. Solar Cells 65 (2001) 171.
[16] X.H. Liu, J. Yang, L. Wang, X.J. Yang, L.D. Lu, X. Wang, Mater. Sci. Eng. A: Struct. Mater. Properties, Microstruct. Process. 289 (2000) 241.
[17] K. Kajihara, T. Yao, J. Sol–Gel Sci. Technol. 16 (1999) 257.
[18] J. Matos, J. Laine, J.M. Herrmann, J. Catal. 200 (200) 10.
[19] T.C. Rojas, M.J. Sayagués, A. Caballero, Y. Koltypin, A. Gedanken, L. Ponsonnet, B. Vacher, J.M. Martín, A. Fernández, J. Mater. Chem. 10 (2000) 715.